

THERMAL DESIGN OF REFRIDGERATED HEXAPOLE 18 GHZ ECRIS HIISI

T. Kalvas, O. Tarvainen, H. Koivisto, K. Ranttila

University of Jyväskylä, Department of Physics, 40500 Jyväskylä, Finland

Abstract

A project is underway for constructing a new 18 GHz ECR ion source HIISI at University of Jyväskylä. An innovative plasma chamber structure with grooves at magnetic poles for larger chamber radius at poles. The hexapole will be refrigerated to sub-zero temperatures to boost the coercivity and the remanence of the permanent magnet material and to allow the use of high remanence, low intrinsic coercivity permanent magnet materials. The hexapole structure is insulated from high temperature solenoid coils and plasma chamber by vacuum. The thermal design of the structure has been made using a thermal diffusion code taking in account radiative, conductive and convective heat transfer processes. The heat flux distribution from plasma has been estimated using electron trajectory simulations. The electron simulations are verified by comparing the distribution to plasma chamber patterns from 14 GHz ECR. Thermal design efforts are presented together with an analysis of the demagnetizing H-field in the permanent magnets.

INTRODUCTION

A project is underway for constructing a new 18 GHz ECR ion source HIISI at the University of Jyväskylä. The minimum-B magnetic field configuration is created by normally-conducting solenoid coils and permanent magnet 24-segment Halbach-array hexapole. See figure 1 for a schematic presentation of the ion source and the magnetic field. An innovative plasma chamber structure with grooves at magnetic poles is being studied [1]. This allows large chamber radius at the poles, leading to the pole field necessary according to the scaling laws while using less permanent magnetic material than a conventional design would. The smaller radius between the poles makes space for chamber water cooling. The hexapole will be refrigerated to sub-zero temperatures to boost the coercivity and the remanence of the permanent magnet material. The hexapole structure is insulated from high temperature solenoid coils and plasma chamber by vacuum. See figure 2 for a cross section view of the ion source. The overall design of the ion source is presented elsewhere in detail [1], while this paper concentrates on the thermal modelling and engineering choices of the plasma chamber and the refrigerated hexapole and the analysis of the demagnetizing H-field in the permanent magnet structure.

ELECTRON TRAJECTORY SIMULATIONS

An estimate of the heat flux distribution from the ion source plasma to the plasma chamber wall is needed for

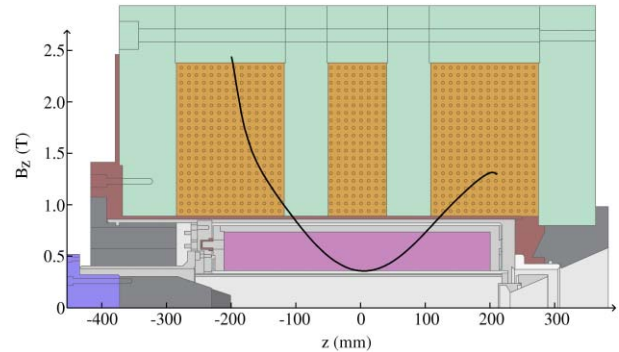


Figure 1: Schematic presentation of the 18 GHz ECRIS HIISI with the axial magnetic field overlaid.

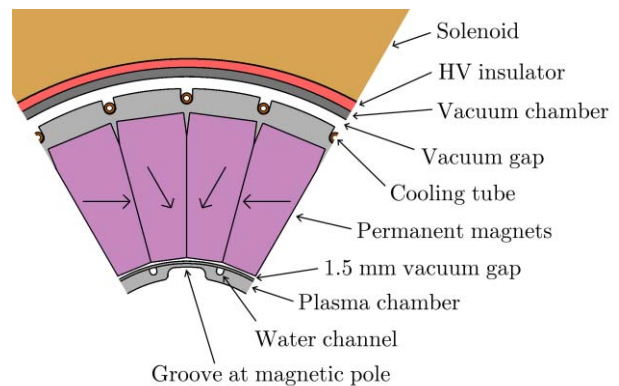


Figure 2: Cross section of the 18 GHz HIISI showing part of the refrigerated 24-segment Halbach permanent magnet hexapole and the vacuum gaps insulating it from the plasma chamber and the solenoid coils. The plasma chamber is grooved to increase the radius at the pole.

credible thermal studies of the plasma chamber and the permanent magnets. A computer code was devised for this purpose. The code tracks single electron trajectories in the ion source magnetic field using relativistic energy-conserving leapfrog-type Boris algorithm [2]. Electric fields and plasma processes are not considered. The particles are launched isotropically from random locations fulfilling the condition $B < B_{\text{ecr}}$, where B_{ecr} is the resonance field for relativistic electrons with kinetic energy E . Thus, the simulated trajectories can be thought to represent electron trajectories after a collision process in the plasma. If the particle is in the loss-cone it will escape the magnetic bottle in a finite time and contribute to the heat flux on the plasma chamber. Otherwise it will remain confined in the plasma.

Magnetic Field Model

The magnetic field used in the simulations is a superposition of analytic models for the solenoid field in (r, z) coordinates and the hexapole field in (r, θ) coordinates. The solenoid field model is constructed by fitting a sixth order polynomial $B(z)$ to on-axis magnetic field data from FEMM simulation [3] from the bias disc to the plasma electrode. The evaluation of the solenoid field at off-axis locations is done using standard expansion, presented for example in [4]. The hexapole field model is constructed by fitting a linear combination of cylindrical multipoles

$$B(r, \theta) = \sum J \left(\frac{r}{r_{\text{ref}}} \right)^{-1} \cos(i\theta) \quad (1)$$

$$B(r, \theta) = \sum -J \left(\frac{r}{r_{\text{ref}}} \right)^{-1} \sin(i\theta) \quad (2)$$

to FEMM simulation field data. The parameters J_1, J_2, J_4, \dots are zero due to hexapole symmetry. Therefore a six-parameter fit is acquired by fitting the non-zero parameters $J_3, J_9, J_{15}, J_{21}, J_{27}$ and J_{33} . The reference radius r_{ref} corresponds to the plasma chamber radius at the pole (38 mm in case of JYFL 14 GHz ECRIS and 55 mm in case of 18 GHz HIISI).

Validation

The electrons are tracked until their trajectories intercept with the plasma chamber or the maximum tracking time of 1000 ns has elapsed. On average 70 % of the particles are time-limited when the electron energy is below 200 keV. Increasing the tracking time by a factor of 10 decreases the number of time-limited particles by less than 1 % (see figure 3). Therefore it seems that majority of the time-limited electrons are not in the loss cone of the magnetic field configuration. It is assumed that the electrons escaping the plasma during this time represent the electron flux of much longer tracking times with appropriate accuracy. Time-step $\Delta t = 1$ ps is used for the trajectory calculation. A few trajectories were studied in more detail and it was observed that the accumulation of error in the particle location is less than 1 mm during 1000 ns.

The code was first used to acquire the electron flux distributions to the plasma chamber of the JYFL 14 GHz ECRIS [5] (see table 1 for the characteristic numbers of the magnetic field) with electron kinetic energies of 10, 100 and 200 keV to test the validity of the simulation. At kinetic energy higher than 200 keV the ECR surface starts intersecting with the plasma chamber wall between the magnetic poles. In each case the number of simulated particles was 10^6 . The distribution of electron fluxes in the simulations are presented in table 2 in percentages. A comparison of the electron flux distributions acquired with the simulations for radial direction against experimental results is presented in figure 4. The figure 4a shows a photograph [6] of an aluminium liner placed inside the plasma chamber during beam production with the MIVOC-method [7]. The carbon

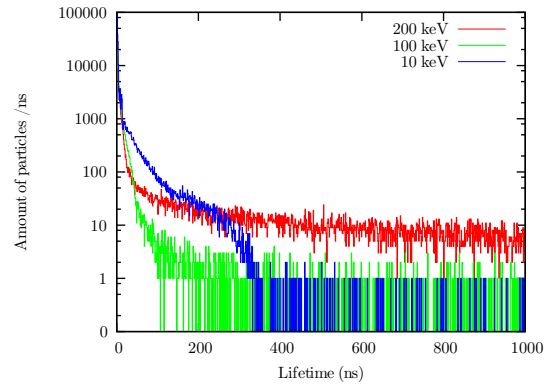


Figure 3: The lifetime of electrons in the electron trajectory simulations with the JYFL 14 GHz ECRIS magnetic field.

contaminants have left black marks at the poles, which are encircled by the red line in the figure. The same encircling has been transferred to the figures illustrating the electron tracking results to enable comparison of the flux patterns. It can be seen that the observed marks match well with the electron flux distribution with kinetic energy of 200 keV and that all the simulated patterns are within the observed marks. Even though the the observed marks are left by ions and the simulation tracks electrons, the comparison gives confidence in the simulations because it is known that ions and electrons occupy roughly the same spatial coordinates in ECRIS.

Table 1: Characteristics of the magnetic fields used in electron simulations. The 14 GHz ECRIS field corresponds to the typical operating point with 520 A solenoid currents.

	14 GHz ECRIS	18 GHz HIISI
B_{min}	0.37 T	0.36 T
B_{inj}	2.03 T	2.43 T
B_{ext}	0.94 T	1.31 T
B_{pole}	1.08 T	1.29 T
B_{btw}	0.69 T	0.95 T

18 GHz HIISI ECRIS

The electron trajectory code was also used to acquire flux distributions for the 18 GHz HIISI ECRIS being designed (characteristic numbers of the magnetic field are presented in table 1). The flux distributions to different parts of the plasma chamber are presented in table 2. The radial flux patterns show similar characteristics as in the 14 GHz ECRIS case. The flux of higher energy electrons covers a wider area around the pole. 10 keV electrons are confined to an area ± 5.5 mm around the pole, 100 keV electrons to ± 9.4 mm and 200 keV electrons to ± 12.7 mm. The grooves in the plasma chamber are ± 8 mm wide. In the thermal modelling of the ion source it is important to consider the worst case scenario for the system. Therefore the 10 keV case with the highest electron flux density in the radial direction has been chosen as an input for the thermal model.

Table 2: Distribution of electron fluxes to different parts of the plasma chamber in simulations in percentages. The flux to the 8 mm diameter extraction aperture is also included in the total flux to the extraction end of the plasma chamber.

	Flux in 14 GHz ECRIS	Flux in 18 GHz HIISI
	10 / 100 / 200 keV	10 / 100 / 200 keV
Injection flux	8.3 / 6.9 / 5.7	6.7 / 5.7 / 5.1
Extraction flux	27.1 / 23.5 / 22.6	12.4 / 10.4 / 9.1
Extraction aperture flux	5.1 / 3.4 / 2.6	2.2 / 1.5 / 1.0
Radial flux	64.5 / 69.7 / 71.7	80.8 / 83.9 / 85.8

The amount of power used to heat the plasma is estimated to be 6 kW at highest. According to the 10 keV simulation, the injection (bias plate) will receive a 400 W flux and the extraction a 750 W flux. These parts will be water cooled. The radial direction is more critical due to the refridgerated hexapole. Therefore this direction is analyzed more carefully. To gain some safety margin it is assumed that all of the 6 kW power is deposited radially to the plasma chamber. With this assumption 10 keV simulation yields the power density distribution shown in figure 5.

THERMAL MODELLING

The thermal modelling for the ion source parts is done in 3D using a computer code, which solves the discretized heat transfer problem in a Cartesian grid with a regular step size. The code takes in account conductive, radiative and convective processes and is capable of handling different materials with non-linear thermal conductances, heat capacities, mass densities, emissivities, absorptivities, etc. The radiative and convective transfer models assume thin gaps, which means that heat transfer takes place only in the direction of the surface normal. Therefore no dispersion of heat flux takes place. This approximation slightly emphasizes localized heat loads.

Plasma Chamber

The plasma chamber of the HIISI ECRIS is going to be constructed from two concentric aluminium cylinders. The ± 8 mm grooves in the inner surface and the flow channels for the cooling water are machined to the inner cylinder. The outer cylinder is shrink fitted onto the inner cylinder to enclose the water channels. The cylinders are welded together at the ends. See figure 6 for a cross section view of the plasma chamber. Based on tests with similar structures, a thermal contact resistance of around $8000 \text{ W}/(\text{m}^2\text{K})$ is expected between the cylinders.

The temperature distribution of the plasma chamber has been calculated assuming the heat flux from the plasma shown in figure 5 and radiative and convective heat exchange with the surrounding hexapole structure at 263 K (-10°C). The water in the cooling channel is at 300 K. The highest temperatures of 405 K appear at the inner surface of the chamber at $z = 25$ (see figure 1 for the coordinates) as shown in a cross section view in figure 6. At the outer surface with a line-of-sight to the hexapole up to 360 K tem-

peratures are observed. Therefore, it is critical to prevent contact between the hexapole magnets and the plasma chamber to avoid demagnetizing the permanent magnets. Careful engineering is required as the gap between the plasma electrode and the hexapole structure is nominally only 1.5 mm.

Refridgerated Hexapole

The Halbach-array hexapole is constructed inside a cylindrical aluminium shell with machined grooves on the outer surface for copper tubes with liquid coolant nominally at 263 K. At the ends of the cylindrical structure, the permanent magnets are confined by aluminium plates, which are bolted to the shell. This whole structure is under rough vacuum to minimize convective heat transfer with the other parts. It is expected that < 1 Pa is reached and therefore 1 Pa and 10 Pa cases have been simulated. The radiative heat transfer is a function of surface emissivities. In the simulations, the emissivity has been assumed to be same for all surfaces. The simulations have been done with 0.1, 0.5 and 1.0 emissivities. According to the material datasheets, it is expected that the surface emissivities are below 0.5, but the unity emissivity case is simulated as a worst case scenario. The permanent magnet structure is held in place by 6 PEEK insulated supports at each end, which are connected to plates at 300 K. These supports are the only conductive heat transfer channel from the hexapole transferring about 12 W of power in total. The vacuum tank surrounding the hexapole in the radial direction is assumed to be at 320 K due to the heat load of the surrounding solenoid.

A cross section view of the temperature distribution at the center of the hexapole ($z = 0$ mm) is shown in figure 7 for the worst case with 10 Pa pressure and 1.0 emissivity. The peak temperature is only 3 K higher than the coolant temperature. Therefore it is believed that there is margin for imperfections in the system as long as there is no contact between the hexapole and the surrounding parts other than the supports.

The thermal model assumes perfect contact between the magnets, which may not be the case in reality, but this is not be a problem because most of the heat flows radially from the inner surface towards the cooling circuit. It is more critical that a good thermal contact is ensured between the magnets and the aluminium cylinder. Therefore, the use of

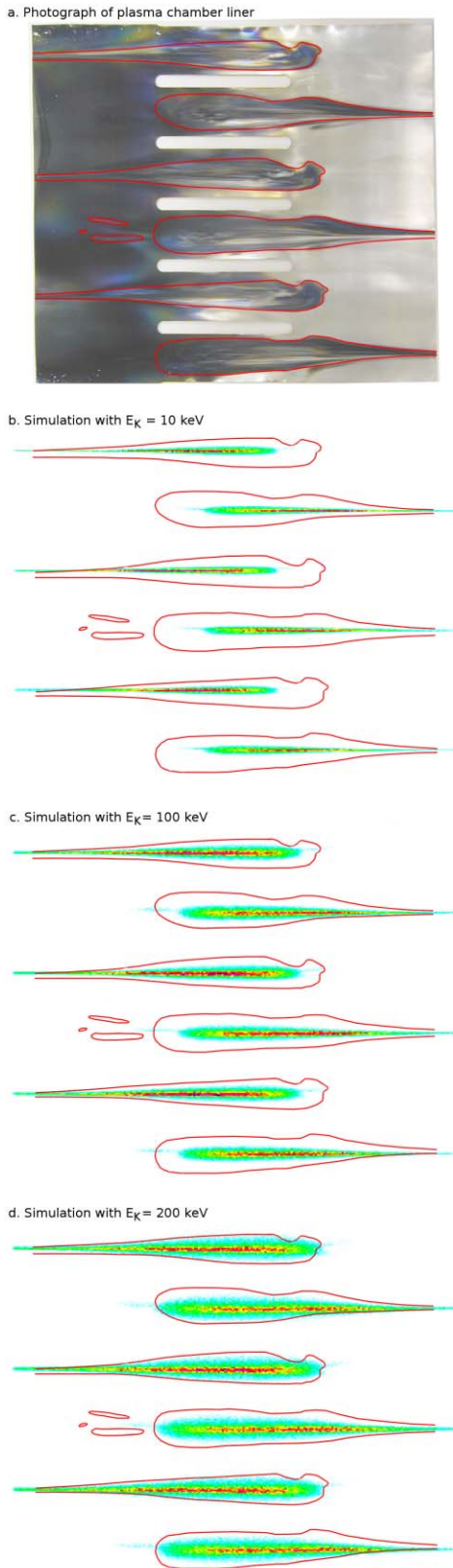


Figure 4: Comparison of the simulated electron fluxes to the marks left by carbon contaminants on the JYFL 14 GHz ECRIS plasma chamber liner.

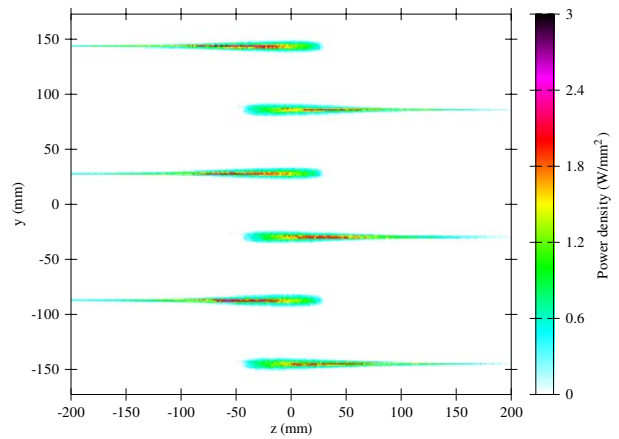


Figure 5: Power density deposited radially on the 18 GHz HIISI plasma chamber assuming 6 kW total power and distribution of the 10 keV electron trajectory simulation.

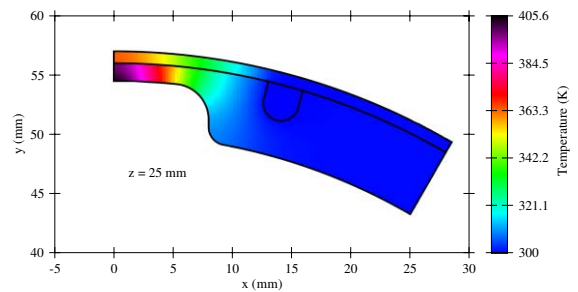


Figure 6: A section view of the plasma chamber temperature distribution.

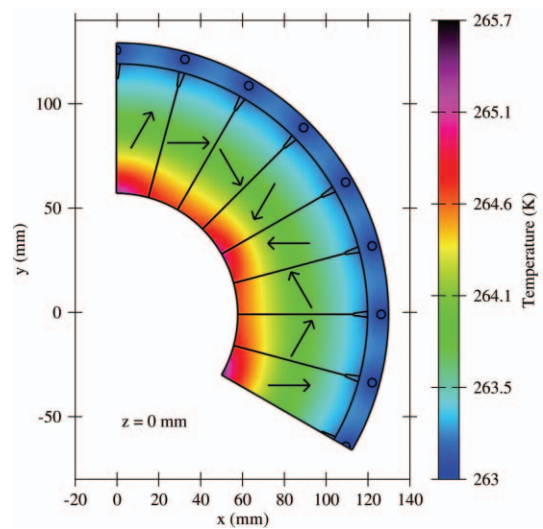


Figure 7: A section view of the hexapole temperature distribution.

Copyright © 2014 CC-BY-3.0 and by the respective authors

vacuum compatible, heat conducting paste at this interface is under consideration.

The required cooling power depends strongly on the pressure and the emissivity of the system. The simulated cooling power requirements for different heat transfer components are presented in table 3. It has been planned that the refridgeration unit will be placed at ground potential, while the hexapole is at +30 kV at highest. The coolant piping needs to be long enough to withstand the potential difference and well insulated to avoid condensation of moisture. It has been estimated that about 15 W will be lost in the transport. For reaching -20°C in $P = 10$ Pa and $\epsilon = 1.0$ conditions a cooling power of 402 W will be needed. Based on this data, a refridgeration unit with at least 300 W cooling capacity at -20°C is being considered even if the nominal design temperature is -10°C .

H-FIELD ANALYSIS

The magnetic field structure has been studied to ensure that the H-field does not cause significant demagnetization of the permanent magnets. The critical limits in different magnet temperatures can be seen in the demagnetization curves in figure 8 for the permanent magnet material N40UH ($B = 1.29$ T and $H = 1990$ kA/m) [8] designed to be used at first in HIISI 18 GHz ECRIS.

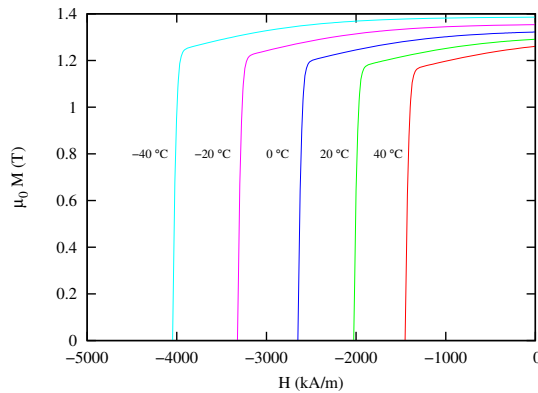


Figure 8: Demagnetization curves for the permanent magnet material N40UH in different temperatures.

The total H-field has been calculated as a superposition of the H-field from two separate 2D FEMM simulations of the hexapole and the solenoid field. Due to symmetries it is sufficient to analyze two of the 12 sectors, which form the 24-segment Halbach hexapole: one with magnetization M pointing inwards and one with M pointing outwards. The resulting 3D H-field maps were separated to field components H_{\parallel} parallel to magnetization and H_{\perp} perpendicular to mag-

$z = 104$ mm planes at which the radial component of the solenoid field is strongest. See figure 9 for colormap representation of the H-field. To avoid the demagnetization at these regions, the permanent magnets should be kept below 20°C . Refridgeration of permanent magnets is therefore not necessary for avoiding demagnetization with the N40UH magnet grade. The refridgeration system makes it possible to use N42SH ($B = 1.32$ T and $H = 1600$ kA/m) and N48H ($B = 1.42$ T and $H = 1350$ kA/m) grades [8].

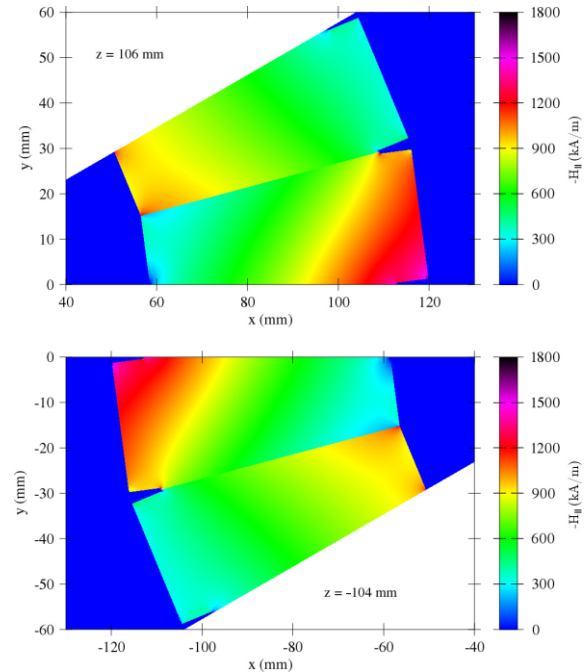


Figure 9: Colormap representation of $-H_{\parallel}$, the H-field component opposing the magnetization.

netization. The H_{\perp} values are less than 1600 kA/m everywhere. According to [9] the resistance to demagnetization in the perpendicular direction is almost double that compared to the parallel direction. Therefore the H_{\perp} will not cause any problems at permanent magnet temperatures less than 50°C . The largest negative H_{\parallel} values are 1800 kA/m, which are encountered in the hexapole at $z = -106$ mm and

ACKNOWLEDGMENTS

This work has been supported by the EU 7th framework programme “Integrating Activities — Transnational Access”, project number: 262010 (ENSAR) and by the Academy of Finland under the Finnish Centre of Excellence Programme 2012–2017 (Nuclear and Accelerator Based Physics Research at JYFL) and Research Infrastructure Programme of the Academy of Finland.

Table 3: Heat flux components and total cooling power needed for reaching -10°C with different pressures P and emissivities ϵ . The numbers do not include 15 W loss in piping outside the ion source.

	$P = 1$ Pa $\epsilon = 0.1$	$P = 1$ Pa $\epsilon = 0.5$	$P = 10$ Pa $\epsilon = 0.1$	$P = 10$ Pa $\epsilon = 0.5$	$P = 10$ Pa $\epsilon = 1.0$
Radiative	19.7 W	98.3 W	19.6 W	98.0 W	195 W
Convective	16.0 W	16.0 W	159 W	159 W	158 W
Conductive	12.0 W	12.0 W	12.0 W	12.0 W	12.0 W
Total	47.7 W	126 W	191 W	268 W	365 W

REFERENCES

- [1] H. Koivisto, et. al., in these proceedings.
- [2] J. P. Boris, Proceedings of the 4th Conference on the Numerical Simulation of Plasmas, Naval Research Laboratory, Washington D. C., 2–3 November 1970, pp. 3–67.
- [3] D. C. Meeker, Finite Element Method Magnetics, Version 4.0.1. (3 Dec 2006 build), <http://www.femm.info/>.
- [4] J. Rodney and M. Vaughan, IEEE Trans. Electron Devices **19**, 144 (1972).
- [5] H. Koivisto, et. al., Nucl. Instrum. Meth. B **174**, 379 (2001).
- [6] P. Suominen, “Modified Multipole Structure for Electron Cyclotron Resonance Ion Sources”, Ph. D. Thesis, Department of Physics, University of Jyväskylä, Research Report No. 6/2006.
- [7] H. Koivisto J. Ärje and M. Nurmia, Nucl. Instrum. Meth. B **94**, 291 (1994).
- [8] Xiamen Dexing Magnet Tech. Co. Ltd., “Magnetic Properties of Sintered NdFeB Magnets”, <http://www.magneticalloy.com/sintered-NdFeB-magnet.htm>
- [9] S. Ruoho et. al., IEEE Trans. Magnetics **44**, 1773 (2008).